Applied Geography 45 (2013) 119–130

Contents lists available at ScienceDirect

Applied Geography

journal homepage: www.elsevier.com/locate/apgeog

Geographical and seasonal variability of the global "practical" wind resources

Cristina L. Archer [a,*], Mark Z. Jacobson [b]

[a] College of Earth, Ocean, and Environment, University of Delaware, Newark, DE 19716, USA
[b] Department of Civil and Environmental Engineering, Stanford University, Stanford, CA 94305, USA

Keywords:
Wind power
Wind energy
Wind
Numerical modeling
Capacity factor

A B S T R A C T

This paper provides global and seasonal estimates of the "practical" wind power obtained with a 3-D numerical model (GATOR-GCMOM) that dynamically calculates the instantaneous wind power of a modern 5 MW wind turbine at 100-m hub height at each time step. "Practical" wind power is defined as that delivered from wind turbines in high-wind locations (year-average 100-m wind speed $\geq$ 7 m/s) over land and near-shore, excluding both polar regions, mountainous, and conflicting land use areas, and including transmission, distribution, and wind farm array losses. We found that seasonal variations in the global practical wind resources are significant. The highest net land plus near-shore capacity factors globally are found during December–January–February and the lowest during June–July–August. The capacity factors in the transitional seasons (March–April–May and September–October–November) are rather similar to one another in terms of geographical patterns and frequency distributions. The yearly-average distributions of capacity factors, whether in terms of geographic patterns or frequency distributions, differ from those in all four seasons, although they are closest to the transitional seasons. Regional practical wind resources are sensitive to seasons and to thresholds in year-average wind speed and bathymetry, but are more than enough to supply local electricity demand in all regions except Japan.

Introduction

Wind energy is expected to play a major role in the transition from finite and polluting energy sources – fossil and fissile fuels – to a clean, sustainable, and renewable energy infrastructure (Jacobson & Delucchi, 2011). Although it is known that the global wind resource is large (Archer & Jacobson, 2005; Cho, 2010; Grubb & Meyers, 1993; Hoogwijk, de Vries, & Turkenburg, 2004; Lu, McElroy, & Kiviluoma, 2009), the exact magnitude of extractable wind power worldwide is still under debate, mainly for four reasons: 1) the definitions and assumptions used in calculating global wind power are often inconsistent; 2) wind speed observations at the hub height of modern wind turbines ($\sim$100 m) are few and sparse; 3) global model maps evaluated against data are not available at high-resolution, either spatially or temporally; and 4) the feedbacks between the wind farms and the regional- and large-scale atmospheric circulations and climate are just starting to be understood and can cause large reductions in the expected wind power, especially for large installed capacities, of the order of 1 TW ($=10^{12}$ W) or higher (Adams & Keith, 2013; Jacobson & Archer, 2012; Keith et al., 2004; Marvel, Kravitz, & Caldeira, 2012).

The term "wind power potential" is not unequivocal. It can refer to one of four different types of potential, loosely defined here as follows:

- *Theoretical potential*: the maximum theoretical power that can be obtained from wind anywhere on Earth at a given height above ground level (AGL) if no limitations – either technical, practical, or economic – existed. Using petroleum as an analogy, the theoretical wind power potential corresponds to the sum of oil resources (undiscovered prospective, discovered unrecoverable, and discovered sub-commercial) plus discovered oil reserves. Here we adopt the estimate of 255 TW (1 TW = 10^{12} W) at 100 m AGL obtained by Jacobson and Archer (2012), who introduced the concept of "saturation" wind power potential as the maximum wind power that can be extracted (and regenerated by natural processes) upon increasing the number of wind turbines on Earth (over land and oceans), independent of technical feasibility, societal, environmental, or economic considerations, but including climatic feedbacks. This is consistent with Marvel et al.'s (2012) estimate of the theoretical maximum rate of kinetic energy

* Corresponding author. Tel.: +1 3028316640.
E-mail address: carcher@udel.edu (C.L. Archer).

0143-6228/$ – see front matter © 2013 Elsevier Ltd. All rights reserved.
http://dx.doi.org/10.1016/j.apgeog.2013.07.006

extraction of 400 TW (which did not account for actual generation by real turbines).

- *Technical potential*: the portion of the theoretical wind potential that can be extracted with contemporary technologies, i.e., at ~100 m hub-height AGL over land and over shallow, near-shore water and including limitations due climate feedbacks, minimum and maximum wind speeds allowed for operating a turbine, and array, transmission, and distribution losses. The only estimate of the land plus near-shore technical wind power potential that includes climate feedbacks to date is 80 TW (Jacobson & Archer, 2012). This was obtained from wind turbines spread everywhere on land and near-shore except over polar regions.
- *Practical potential*: the portion of technical wind power potential that can be harvested after excluding areas with practical restrictions (such as conflicting land and water uses or remoteness) and adopting common practices (such as installing wind farms only at sufficiently-windy locations). No evaluation of the practical wind power potential that includes climatic feedbacks exists in the literature. Even though the bottom-up method of summing up wind power output at individual locations over large regions is acceptable as long as the global wind power generation over land remains lower than ~40 TW (Jacobson & Archer, 2012), the practical potential at the global scale would exceed 40 TW if calculated with the bottom-up method and therefore it will not be calculated in this study. The global practical wind power potential is expected to be lower than 80 TW (Adams & Keith, 2013). Previous estimates that did not account for climate feedbacks varied between 11 and 96 TW (Archer & Jacobson, 2005; Hoogwijk et al., 2004; Lu et al., 2009). By comparison, the global electricity demand in 2012 was 2.44 TW (International Energy Agency, 2012).
- *Economic potential*: the portion of practical wind power potential that can be harnessed as a function of actual production costs. Generally speaking, only a fraction of the practical potential can be extracted at the lowest cost, as land, political, and social/environmental constraints increase the final production cost (Hoogwijk et al., 2004). The economic potential can only be determined based on an analysis of ever-varying factors such capital cost, production cost, electricity prices, and salient policies such as the Production Tax Credit and feed-in tariffs. These factors are beyond the scope of this study.

Although the need for clear definitions of wind power potentials has been addressed (GEA, 2012; Hoogwijk et al., 2004), consistency in the definitions is still lacking in the literature and estimates of wind power potentials can vary by orders of magnitude. Since the practical potential is possibly the most relevant, objective, and insensitive to market fluctuations, it and its seasonal variations are the primary foci of this study.

The global practical wind power potential is difficult to map accurately because worldwide wind speed measurements are not available at the hub height of modern wind turbines (~100 m). As such, vertical interpolations and extrapolations of measurements over hundreds of meters of altitude have been proposed, such as the Least Square Error method (Archer & Jacobson, 2003, 2005) or the log- and power-laws (Arya, 1988; Burton, Sharpe, Jenkins, & Bossanyi, 2001). These techniques can be applied to both measurements and model results, but are approximate because they are based partly on theoretical and partly on empirical considerations (Arya, 1988). In this study, this limitation is overcome by using a 3-D atmospheric model with multiple layers in the boundary layer, including two layers with centers close to 100 m, allowing for a nearly precise model estimate of 100-m AGL wind speeds.

Global maps of the wind resource at hub height are not available at horizontal and temporal resolutions that are fine enough to resolve significant local wind features or seasonal and monthly fluctuations of the global wind resource. Observation-based hub-height wind estimates, such as in Archer and Jacobson (2005), are limited by the sparse data in most regions of the globe. Fine-resolution hub-height wind maps are available for certain regions, such as the U.S. West and East Coasts (Dvorak, Archer, & Jacobson, 2010; Dvorak, Stoutenburg, Archer, Kempton, & Jacobson, 2012), but not for the world, due to practical computational limitations. The ERA-Interim reanalyses (Dee, Uppala, & Simmons, 2011) are currently available at 0.8° resolution with continuous data assimilation, which ensures proper sea surface temperature and no spurious climate shift; however, this product is available at low temporal resolution (6 h) and not freely. Another observation-based study (Capps & Zender, 2010) examines the seasonal cycle of wind power at high (0.25°) resolution, but only over the oceans.

No study to date has addressed the seasonal and monthly fluctuations of practical wind power on the global scale. This study addresses both issues – horizontal/vertical spatial resolution and temporal resolution – by providing relatively fine-resolution maps of seasonal and annual global practical wind power (and other relevant parameters). A limitation of this study is that topography is not resolved below 1.5° horizontal resolution. However, the model does treat sub-grid soil and land use classes and calculates surface energy and moisture fluxes over each sub-grid soil class at every model time step. Running global simulations at higher-resolution than was done here was not possible given the complexity of the model and the computational resources available for this study.

Methods

The model used for this study is GATOR-GCMOM, a one-way-nested (feeding information from coarser to finer domains) global-to-regional Gas, Aerosol, Transport, Radiation, General Circulation, Mesoscale, and Ocean Model that simulates climate, weather, and air pollution from the global to local scale. The model has been evaluated previously (Jacobson, 2001, 2010; Jacobson & Streets, 2009) and processes within it have also been compared with those in other coupled climate-air pollution models (Zhang, 2008).

For this study, the global-domain simulations were run at three horizontal resolutions: 4° × 5°, 2° × 2.5°, and 1.5° × 1.5° latitude and longitude (Table 1). Initial conditions for each simulation were obtained with 1ox1o reanalysis fields (GFS, 2010). To eliminate the effects of the initial state, results for the first several months of each simulation were discarded and only results from 2007 were retained. The model treated 47 vertical layers up to 60 km, including 15 layers in the bottom 1 km. The four lowest levels were centered at approximately 15, 45, 75, and 106 m above the ground, but the heights of such centers changed continuously in a small range since the vertical coordinate system used was the sigma-pressure coordinate. At each time step, though, all wind speeds were interpolated vertically between two layer centers to exactly 100 m, the hub height of the wind turbine assumed for the calculations here.

The model solves the momentum equation with the potential-enstrophy-, vorticity-, energy-, and mass-conserving scheme of

Table 1
Details of the global simulations run for this study.

Run name	Horizontal resolution	Time step (s)	Start date	End date
4 × 5	4° SN × 5° WE	30	1 Jan 2006	31 Dec 2009
2 × 2.5	2° SN × 2.5° WE	30	27 Aug 2005	31 Dec 2009
1.5 × 1.5	1.5° SN × 1.5° WE	30	19 Feb 2006	31 Dec 2008

Arakawa and Lamb (1981). Two-dimensional ocean mixed-layer dynamics conserves the same four properties while predicting mixed-layer velocities, heights, and energy transport (Ketefian & Jacobson, 2009). The model solves 3-D ocean energy and chemistry diffusion, 3-D ocean equilibrium chemistry, and ocean-atmosphere exchange. The model also treats sub-grid soil classes, each with a 10-layer soil model, and surface energy and moisture fluxes separately over each sub-grid class (Jacobson, 2001).

In order to calculate wind power from the model, we first selected the REPower 5M wind turbine (www.repower.de/fileadmin/download/produkte/RE_PP_5M_uk.pdf) for use. With a rotor diameter of 126 m and a hub height of 100 m, it reaches its rated power of 5 MW at the rated speed of $V_{\text{rated}} = 12.5$ m/s. Manufacturer power output data as a function of wind speed were provided only as a graphic curve in one-unit intervals. A third-order polynomial fit was used to obtain wind power output P as a continuous function of 100-m wind speed v:

$$P = av^3 + bv^2 + cv + d. \quad (1)$$

Fig. 1 provides the coefficients a, b, c, and d. No power is produced at wind speeds below 3.5 m/s (cut-in speed) or above 25 m/s (cut-off speed). Because of the change in the curve concavity, different coefficients are provided for low versus high-wind speed.

The dynamical time step in the model was 30 s for all resolutions simulated. During each dynamical time step, the wind speed at 100 m AGL was calculated and used in Eq. (1) to determine the instantaneous wind power at 100 m from a single wind turbine. The ratio of this actual power output to the maximum possible output of 5 MW is referred to as "gross capacity factor" hereafter.

The system efficiency of a wind farm η_S is the ratio of energy delivered to raw energy produced by the turbines. It accounts for array, transmission, and distribution losses (but not for maintenance or availability losses).

Array losses are energy losses resulting from reductions in wind speed that occur in a large wind farm when upstream turbines extract energy from the wind, reducing the wind speed for downstream turbines. Upstream turbines also create vortices or ripples (turbulence) in their wakes that can interfere with downwind turbines. The greater the spacing between wind turbines, the lower the array losses due to loss of energy in the wind, vortices, and wakes. Array losses are generally 5–20% (Frandsen, 2007; Masters, 2005).

Transmission and distribution losses are losses that occur between the power source and end users of electricity. Transmission losses are losses of energy that occur along a transmission line due to its resistance. Distribution losses occur due to step-up transformers, which increase voltage from an energy source to a high-voltage transmission line and decrease voltage from the high-voltage transmission line to the local distribution line. The average transmission plus distribution losses in the U.S. in 2007 were 6.5% (EIA, 2011).

The overall system efficiency of a wind farm, accounting for array, transmission, and distribution losses typically ranges from 0.85 to 0.9; here we assumed an average $\eta_S = 0.875$, corresponding to a system loss of 12.5%. The "net" capacity factor is equal to the gross capacity factor multiplied by the system efficiency.

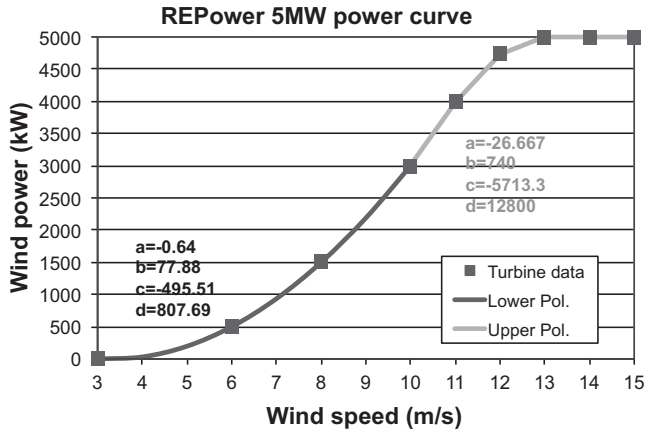

Fig. 1. Power curve of the REPower 5M wind turbine, with coefficients valid for hub-height wind speeds < 10 m/s (lower polynomial, black line) and ≥10 m/s (upper polynomial, gray line), derived from manufacturer's data (www.repower.de/fileadmin/download/produkte/RE_PP_5M_uk.pdf).

Results

Geographic variability of winds

Fig. 2a shows yearly-average 100-m wind speeds during 2007–2008 from run 1.5 × 1.5. The strongest winds are generally found over ocean waters in both hemispheres, noticeably over the Southern Ocean, in the Gulf of Alaska, and the northern Atlantic Ocean. Over land, the windiest locations are the Sahara desert, the Himalayas, the southern tip of South America, and the central regions in North America. Similar findings were obtained from the other two coarse-resolution runs (not shown). Only grid cells in which yearly-average wind speed is ≥7 m/s from Fig. 2a will be used for the practical wind power and capacity factor calculations.

Seasonal patterns of 100-m wind speeds can be dramatically different from those in the yearly-average. For example, the northern Pacific and Atlantic oceans, where the Aleutian and the Icelandic low-pressure systems cause storms and increase wind speeds near the surface in the winter, are characterized by 100-m wind speeds >12 m/s in DJF (December–January–February), but show much weaker winds in JJA (June–July–August). Some regions exhibit strong winds only in a specific season. For example, the localized wind speed maximum offshore of California is a persistent feature in the northeastern Pacific during JJA (Dvorak et al., 2010; Jiang et al., 2008; Liu, Tang, & Xie, 2008) and it represents possibly the greatest summertime offshore wind resource in North America during the season with the highest electric load. This summer wind speed maximum offshore of California is predicted correctly by this model at all resolutions (not shown).

During the transitional seasons MAM and SON (March–April–May and September–October–November), the 100-m wind speed patterns are similar to one another (Fig. 2c and e) and to the yearly-average (Fig. 2a). The finding that the yearly-average distribution somewhat resembles that of the transitional seasons, but not that of winter or summer, will also be confirmed later for net capacity factors, although to a lesser extent.

Mapping the various wind power potentials

This section provides a visualization of the three concepts of theoretical, technical, and practical yearly-average wind power potentials globally. Because the concept of theoretical wind power potential does not depend on a specific turbine model, it is necessary to use the concept of wind power density δ, which is a function of instantaneous wind speed v and air density ρ (assumed to be 1.224 kg/m^3 for the standard atmosphere at 100 m AGL):

$$\delta \equiv \frac{1}{2}\rho v^3. \quad (2)$$

To calculate the yearly-average theoretical wind power density from this instantaneous definition, the Rayleigh wind speed

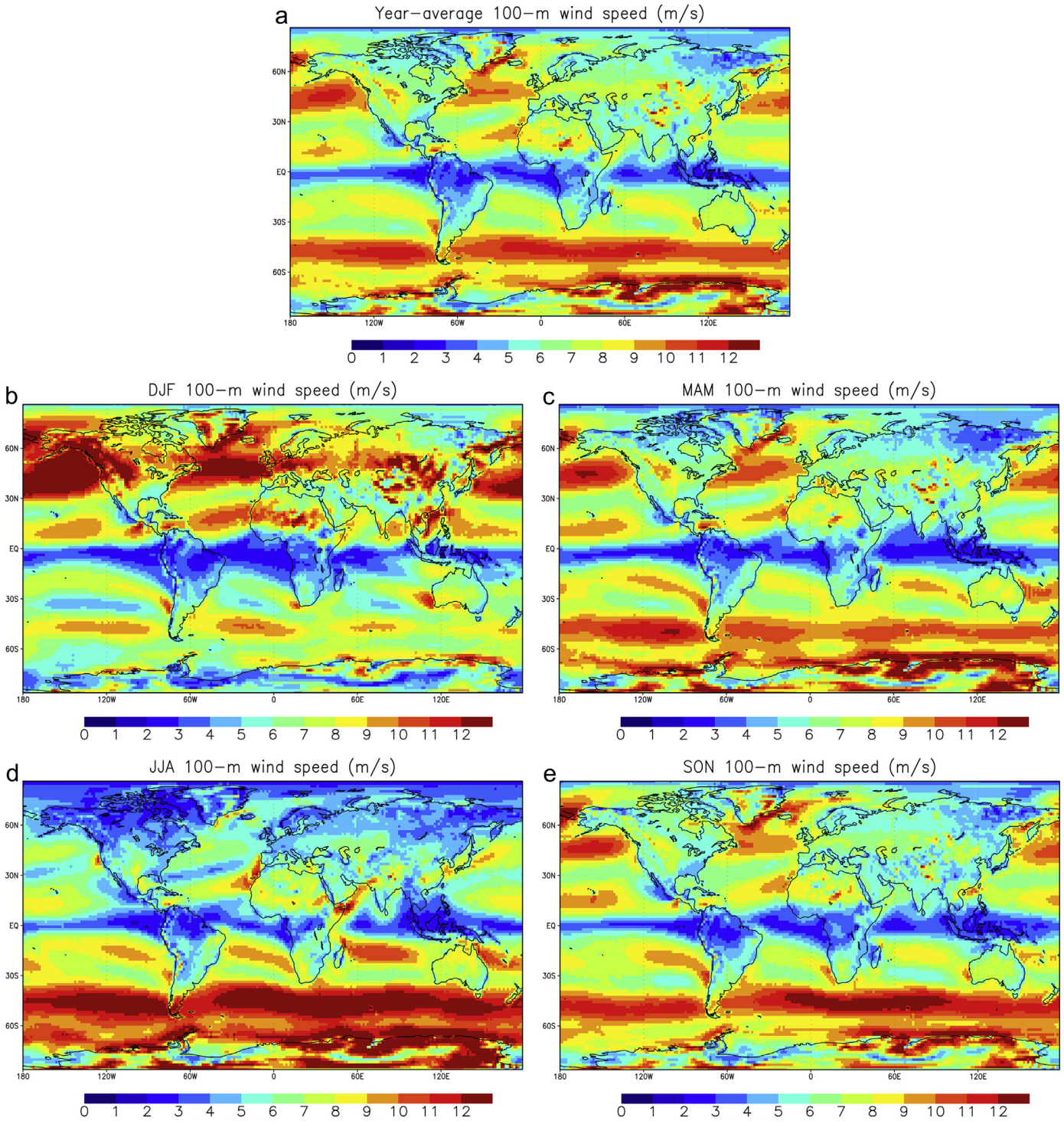

Fig. 2. Distributions of yearly-average (a) and seasonal-average (b–e) wind speed at 100 m in 2007–2008 from run 1.5 × 1.5.

distribution was assumed to obtain the following analytical expression for the yearly-average wind power density $\bar{\delta}$ given the yearly-average wind speed $\bar{v}$:

$$\bar{\delta} = \frac{6}{\pi}\rho\bar{v}^3. \tag{3}$$

Then, the Betz limit (Burton et al., 2001; Masters, 2005) was applied to determine the maximum theoretical wind power density at each grid cell δ_T:

$$\delta_T = \frac{16}{27}\bar{\delta}. \tag{4}$$

This represents the maximum wind power that can be extracted at each grid point for each square meter of turbine swept area perpendicular to the wind and is shown in Fig. 3a. The distribution is obviously strongly influenced by wind speed and closely resembles that in Fig. 2a, because it was derived directly from it.

The concept of technical wind power potential relies on real wind turbines, no longer perfectly efficient at the Betz limit as in the theoretical case. Modern wind turbines installed in areas with average 100-m wind speeds greater than 7 m/s can achieve a gross capacity factor $>$ 40%. By contrast, wind turbines exposed to average wind speeds lower than 7 m/s are less likely to be economically feasible (Jacobson & Masters, 2001), although recent progress in the development of low wind speed turbines may reduce this threshold from 7 to 6.5 m/s in the near future. The turbine power output is first calculated using Eq. (1) and then multiplied by η_S to account for system losses. To allow for a direct comparison with δ_T, the technical wind power was divided by the area swept by the REPower 5M turbine, which is $A_S = \pi D^2/4$, where D is the turbine diameter (126 m), to obtain the technical wind power density δ_C:

$$\delta_C = \frac{\eta_S P}{A_S}. \quad (5)$$

The technical wind power density was only calculated over areas where it is technically possible to install a wind turbine (thus excluding the polar regions, offshore locations deeper than 200 m, and mountainous areas above 2000 m) and is shown in Fig. 3b. Both the areal extent of technical areas, defined as regions over which the technical wind potential can be calculated, and their wind power densities are dramatically reduced with respect to the theoretical case. Because the definition of technical wind power density already accounts for system losses, the technical wind power (W) at a grid cell can be obtained by multiplying Eq. (5) by the area swept by a single turbine and by the number of turbines to be installed in that grid cell.

The practical potential is restricted to windy areas (defined as those with yearly-average 100-m wind speed $\geq$ 7 m/s from Fig. 2a) with no land use conflicts, thus excluding completely grid cells whose land use was either tropical forest, wetland, permanent snow, or urban (Hoogwijk et al., 2004). The definition of practical wind power density δ_P coincides with that in Eq. (5) but is only valid over practical locations, which meet the restrictions listed above. Additional restrictions, described in the next section, may reduce the fraction of a grid cell area that can practically be covered with wind farms (Fig. 4b).

Fig. 3 visually demonstrates how the areas available for wind power extraction shrink as more assumptions and limitations are introduced in the definitions of theoretical, technical, and practical potentials. The general shift in color from red to blue is the effect of using a real, rather than a perfectly efficient, wind turbine. It should be noted that, due to the relative coarse resolution of even the 1.5 $\times$ 1.5 run, Fig. 3c misses many good-wind resource locations that would appear in a higher-resolution map. The present results are designed primarily to estimate resources roughly rather than to give the exact location of resources and to provide a visual aid for the understanding of the three wind power potentials.

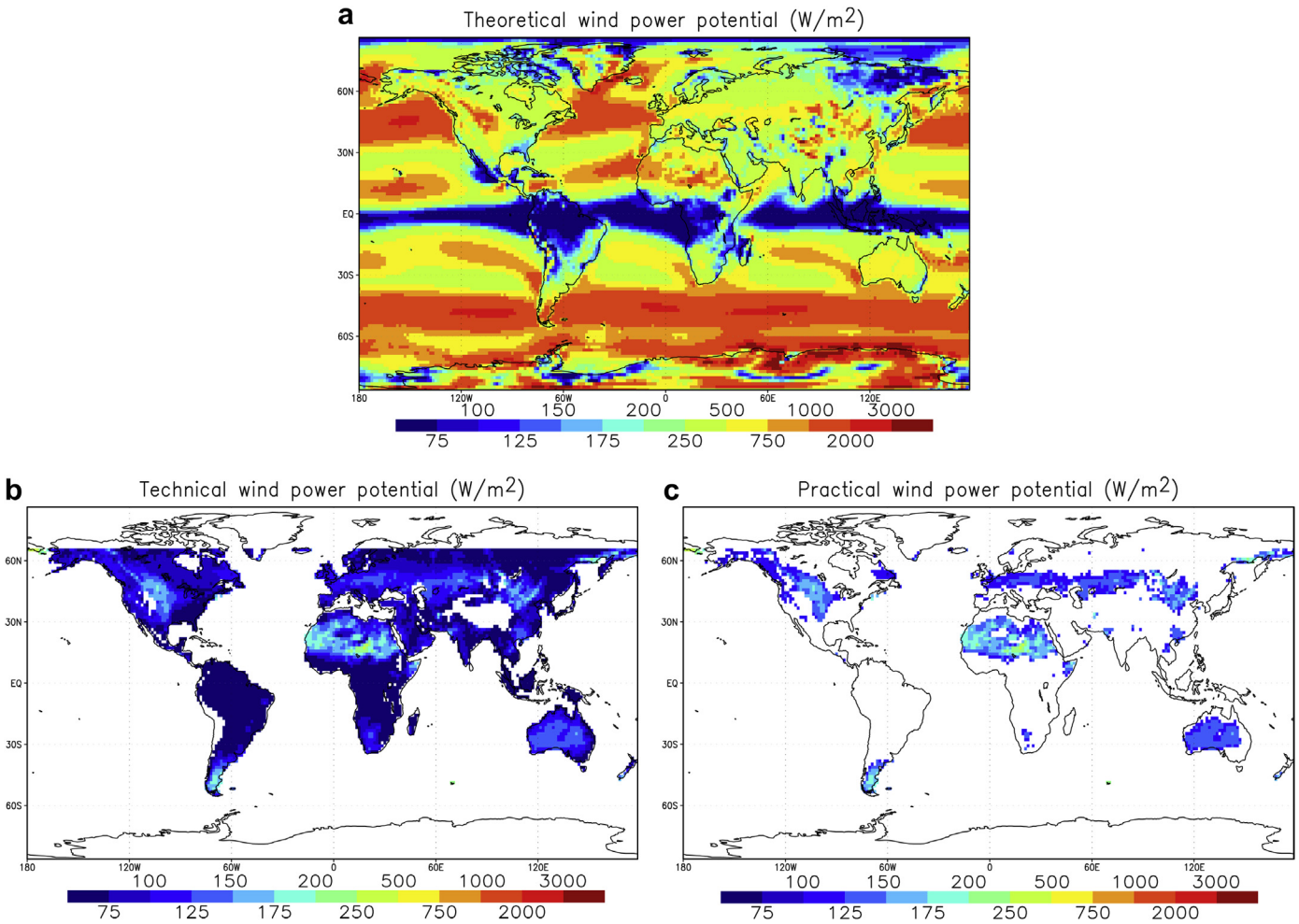

Fig. 3. Global geographical distributions of (a) theoretical, (b) technical, and (c) practical yearly-average wind power densities during 2007–2008. Many good-wind locations over small areas are not resolved at this model resolution (1.5° $\times$ 1.5°). The wind speed threshold in (c) is 7 m/s and the bathymetry is up to 200 m for offshore locations.

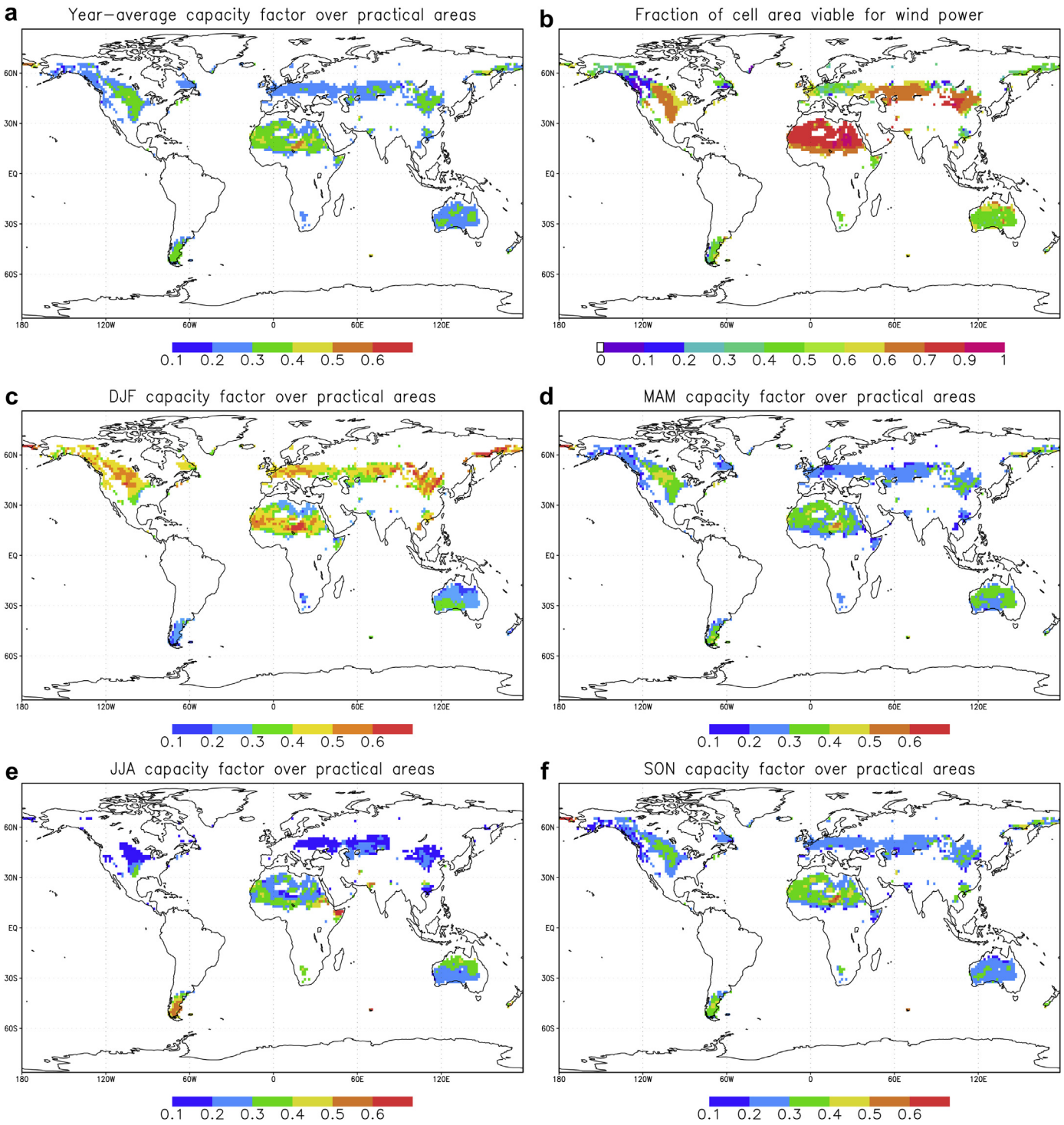

Fig. 4. Average net capacity factor by season (c–f) and yearly (a) during 2007–2008 at "practical" locations (i.e., over land and offshore locations, excluding polar, mountainous, and conflicting land use areas, and with yearly-average 100-m wind speed > 7 m/s) assuming use of the REPower 5 MW wind turbine from run 1.5×1.5. The maximum fraction of each grid cell that could be utilized for wind power extraction is shown in (b).

Distributions of the net capacity factors

Fig. 4 shows the yearly and seasonal-average net capacity factors (during 2007–2008) obtained with the REPower 5M wind turbine for all grid cells over windy land and windy shallow ($\leq$200 m) waters only, considering land use restrictions (described next). Areas with high net capacity factor ($>$0.2) in Fig. 4a are the most desirable for wind power development. Aside from the mid-latitude areas in the Northern Hemisphere, noticeable areas are vast regions in the Sahara Desert and Sahel with an incredible capacity factor of $\sim$0.5.

Fig. 4b shows the maximum fraction of each cell that can be covered with wind farms, assuming the following limitations and assumptions:

- Land and offshore locations with bathymetry < 200 m;
- No regions poleward of 66.56° N and 60° S;
- No mountainous regions above 2000 m of altitude;
- No areas with yearly-average 100-m wind speed lower than 7 m/s;
- Land use limitations are treated as in Hoogwijk et al. (2004) via suitability factors. In brief, tropical forests, wetland, permanent snow, and urban areas are completely excluded (suitability factor of 0%). The following suitability factors are used for other land uses: 100% for deserts and barren land, 90% for savannah, 80% for grassland, 70% for agricultural land, 50% for wooded savannah, and 10% for boreal and temperate forests (Hoogwijk et al., 2004). At offshore locations, a 67% suitability factor is applied, corresponding to the 33% exclusion factor used in Dvorak et al. (2010);
- System losses of 12.5% are included.

In a manner similar to the findings for the global 100-m wind speed distributions, the practical capacity factor can also change dramatically from one season to the next and differ seasonally from the yearly-average distribution (Fig. 4). Because of the larger extent of practical locations over land in the Northern than in the Southern Hemisphere and because the highest winds often occur during the winter, the global wind energy potential appears to be dramatically higher during DJF than during JJA globally. The yellow shades dominate Fig. 4c, suggesting an average capacity factor > 0.4 during DJF over most of the practical areas in the Northern Hemisphere. By contrast, only a few regions in the Southern Hemisphere reach such high capacity factors during JJA (Fig. 4e), mostly limited to Patagonia.

The frequency distributions of the net capacity factors at practical locations season by season are shown in Fig. 5. The yearly-average distribution is remarkably symmetric around the modal bin of 0.25–0.3. No other season exhibits such symmetry. The DJF distribution is skewed toward capacity factors > 0.4, with the mode in the 0.4–0.45 bin. Oppositely, the JJA distribution is skewed toward values < 0.2 and has a rather low modal mode (0.05–0.1). The transitional seasons MAM and SON are again similar to one another, with rather symmetric distributions with high frequencies of the modal values (0.25–0.3) and a narrower shape than the yearly-average distribution. This confirms that the distributions of yearly-averaged wind speed or capacity factor are not similar to those of any particular season.

The horizontal resolution of these simulations is not fine enough to resolve properly some meso- and fine-scale features, such as steep topography or sudden surface roughness or land use horizontal variations, which can enhance local wind speeds. This somewhat coarse resolution, however, is likely to result in an underestimate, rather than an over-estimate, of wind speeds and wind power, as discussed next.

Sensitivity analysis and regional totals

In this section we evaluate the sensitivity of the practical wind power potential to two basic assumptions that were introduced in the previous section: the thresholds for minimum yearly-average 100-m wind speed (7.0 m/s) and for maximum depth for offshore installations (200 m). The previous scenario for practical wind power that was based on these two thresholds will be referred hereafter as the “control scenario”. Reducing the threshold for the

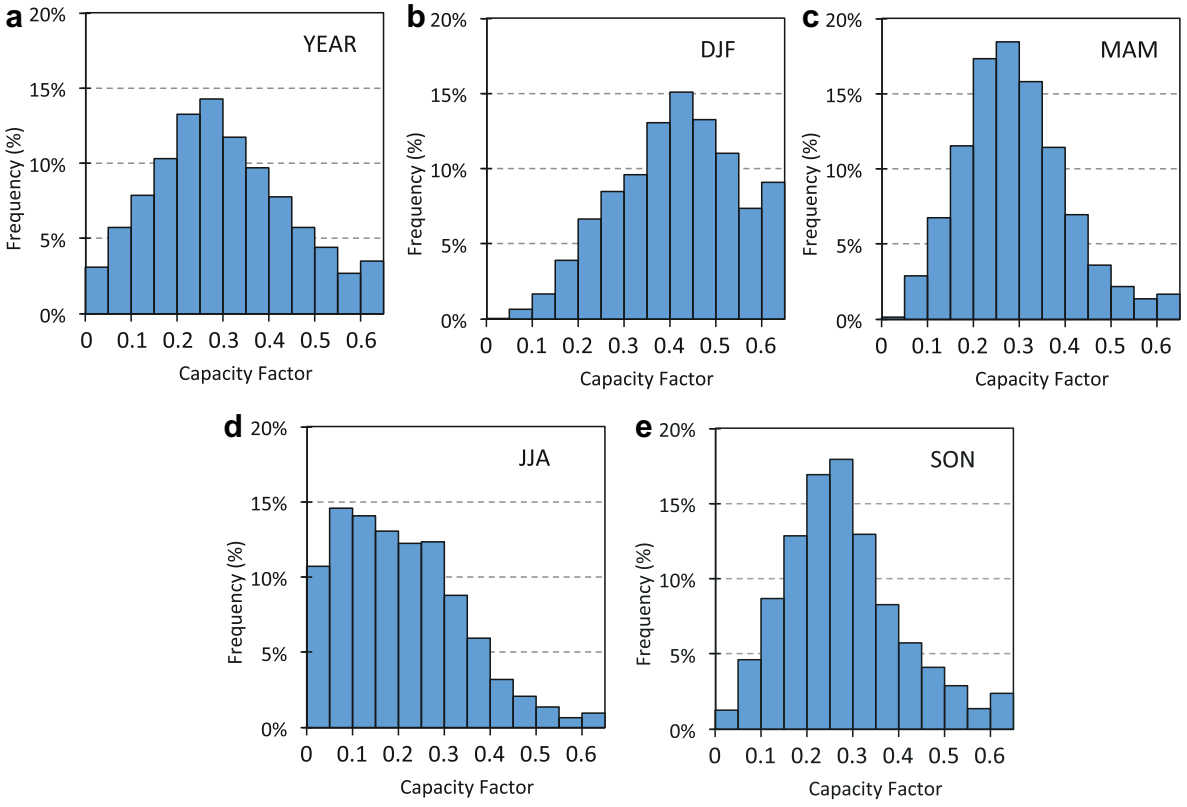

Fig. 5. Frequency distributions of the monthly net capacity factor over “practical” areas (shown in Fig. 4) during: (a) the entire year (2007–2008); (b) DJF; (c) MAM; (d) JJA; and (e) SON. All locations with capacity factors greater than 0.6 are grouped in the last bin in all figures. Frequencies are expressed as number of grid points with capacity factors in each bin over the total number of grid points in practical areas. Seasonal differences are so dramatic that the yearly distribution is not representative of any of the seasonal distributions.

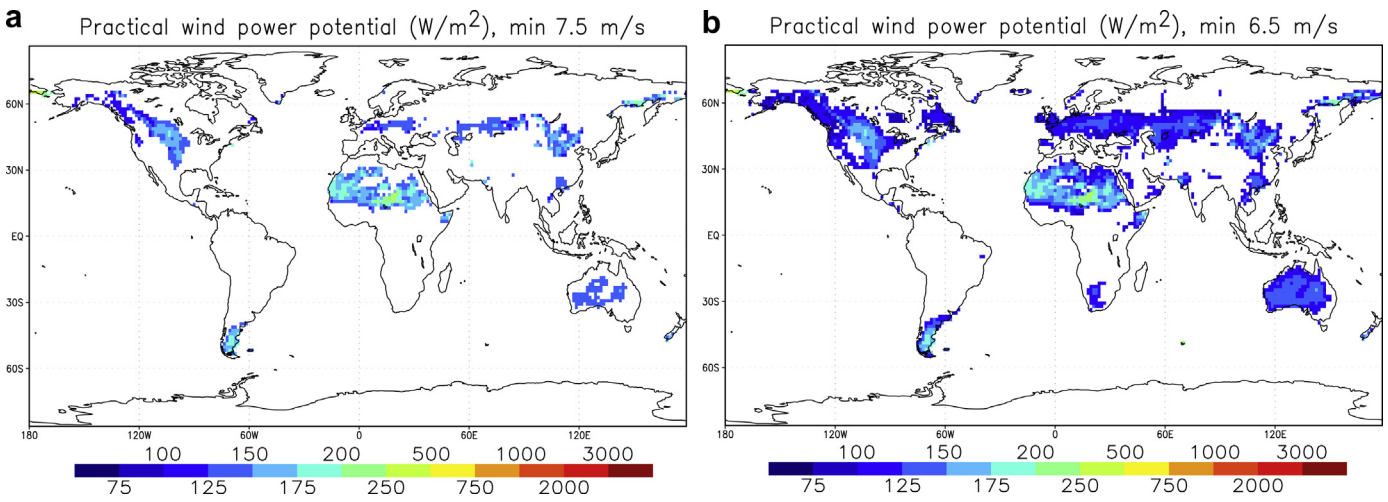

Fig. 6. Maps of the average practical wind power for the low (a) and the high (b) scenarios. In the low scenario (a), areas with average wind speed of 7.5 m/s and with bathymetry up to 100 m for offshore locations were selected; in the high scenario (b), areas with average wind speed of 6.5 m/s and with bathymetry up to 200 m were selected. The control scenario, with a threshold of 7 m/s and bathymetry up to 200 m, is shown in Fig. 3c.

yearly-average wind speed implies that more areas become viable for practical wind power, although at lower efficiencies and capacity factors because the winds are not as strong. Vice versa, increasing the wind speed threshold limits the areas that are practically viable to fewer locations but with higher efficiencies and capacity factors. Similarly, a deeper bathymetry threshold increases the viable areas and vice versa.

A "low scenario" is introduced in which the most restrictive assumptions are used, i.e., shallow bathymetry (up to 100 m only) and very windy locations only (yearly-average wind speed $>$ 7.5 m/s). The "high scenario" instead requires a lower wind speed threshold (6.5 m/s) and a deeper bathymetry (up to 200 m). The control scenario, described before, is an intermediate between the two, with a threshold of 7.0 m/s for wind speed and 200 m for bathymetry. As shown in Fig. 6, the areal extent of the high scenario is larger than that of the intermediate scenario (by $\sim$37%) and much larger than that of the low scenario (by more than a factor of 2), but only due to the addition of marginally productive grid cells (shaded in dark blue, with power densities generally lower than 100 W/m^2). Several offshore locations disappear going from the high to the low scenario.

To quantitatively compare the high, intermediate, and low scenarios, we calculate the regional practical wind power potentials for the regions shown in Fig. 7. Table 2 summarizes the findings by season and by region, on land and offshore, and it includes estimates of the regional electricity consumption rates from IEA (2012) for comparison. In general, all regions have plenty of practical wind resources, especially in Africa. Despite the seasonal variability and the sensitivity to the thresholds in wind speed and bathymetry, in all regions (except in Japan) the practical wind resources, even in the low scenario, are more than enough to cover the local electricity demand.

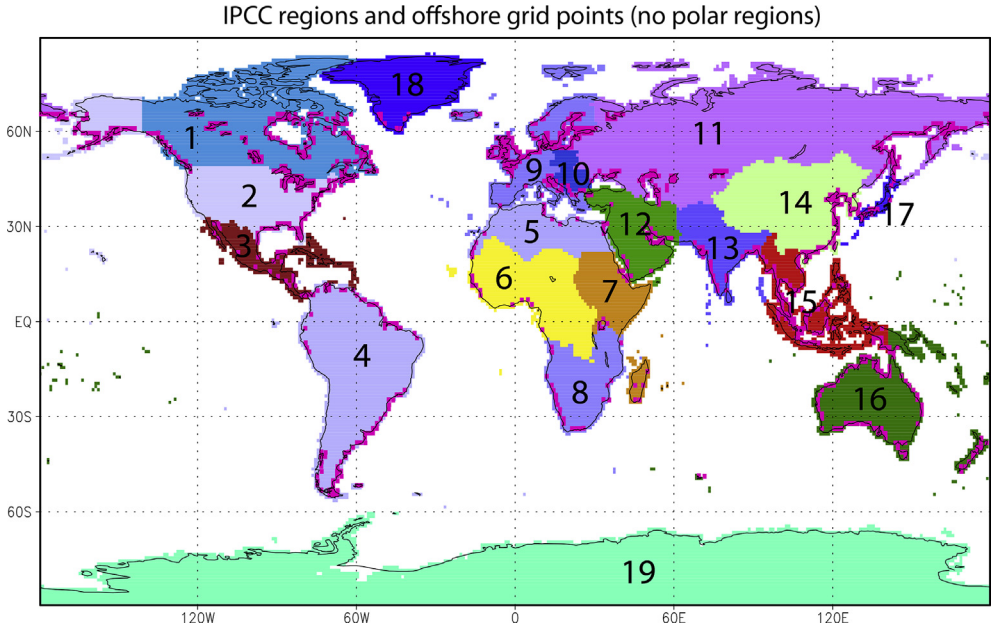

Fig. 7. Map of the 19 regions used in this study and location of offshore grid cells (shaded in shocking pink to enhance readability) with bathymetry $<$ 200 m and soil fraction $\geq$ 5% (excluding both polar regions).

Table 2
Practical wind power potential (in TW) over land and offshore by region (shown in Fig. 7) and by season for the intermediate scenario, with low and high scenario values in parentheses. The total electricity consumption in each region is reported in parentheses below the region names in TW (International Energy Agency, 2012).

Regions and 2010 electricity consumption	DJF			JJA			Year		
	Windy land	Offshore	Total	Windy land	Offshore	Total	Windy land	Offshore	Total
1 Canada (0.059)	4.97 (3.54–6.47)	0.56 (0.06–1.28)	5.53 (3.6–7.75)	0.91 (0.63–1.2)	0.16 (0.01–0.36)	1.06 (0.64–1.56)	3.03 (2.2–3.91)	0.38 (0.04–0.86)	3.41 (2.23–4.77)
2 USA (0.473)	11.67 (8.73–14.12)	0.82 (0.36–1.34)	12.49 (9.09–15.46)	4.47 (3.48–5.49)	0.23 (0.13–0.4)	4.7 (3.61–5.89)	8.29 (6.3–10.05)	0.55 (0.27–0.9)	8.85 (6.57–10.95)
3 Central America (0.034)	0.31 (0.22–0.71)	0.11 (0.02–0.12)	0.42 (0.24–0.84)	0.14 (0.09–0.43)	0.05 (0.01–0.06)	0.19 (0.1–0.49)	0.22 (0.15–0.56)	0.08 (0.01–0.09)	0.3 (0.17–0.66)
4 South America (0.138)	1.37 (1.02–1.71)	0.59 (0.45–0.79)	1.96 (1.46–2.5)	2.42 (2–3.02)	1.07 (0.83–1.36)	3.49 (2.83–4.38)	1.8 (1.43–2.28)	0.78 (0.6–1.02)	2.58 (2.03–3.3)
5 Northern Africa (0.033)	15.25 (11.95–17.42)	0.27 (0.18–0.31)	15.52 (12.13–17.72)	11.66 (8.78–13.18)	0.24 (0.15–0.27)	11.9 (8.93–13.45)	13.42 (10.25–15.27)	0.24 (0.15–0.28)	13.66 (10.4–15.55)
6 Western Africa (0.006)	22.13 (21.17–23.14)	0.08 (0.08–0.08)	22.21 (21.26–23.22)	13.47 (12.62–14.24)	0.04 (0.04–0.04)	13.52 (12.67–14.28)	16.82 (15.97–17.66)	0.07 (0.07–0.07)	16.89 (16.04–17.73)
7 Eastern Africa (0.001)	8.17 (7.3–9.15)	0.02 (<0.01–0.04)	8.19 (7.3–9.19)	7.77 (6.78–8.59)	0.03 (<0.01–0.03)	7.8 (6.78–8.62)	7.12 (6.34–7.92)	0.02 (0–0.03)	7.14 (6.34–7.95)
8 Southern Africa (0.033)	0.65 (0.02–1.3)	<0.01	0.65 (0.02–1.3)	1.22 (0.01–2.4)	<0.01	1.22 (0.01–2.4)	0.86 (0.01–1.73)	<0.01	0.86 (0.01–1.73)
9 OECD Europe (0.317)	3.19 (1.19–4.53)	1.14 (0.19–1.69)	4.33 (1.38–6.23)	0.63 (0.25–0.98)	0.22 (0.05–0.35)	0.85 (0.3–1.33)	1.83 (0.71–2.63)	0.68 (0.12–1)	2.51 (0.83–3.63)
10 Eastern Europe (0.033)	1.32 (1.01–2.16)	<0.01	1.32 (1.01–2.16)	0.34 (0.26–0.67)	<0.01	0.34 (0.26–0.67)	0.77 (0.59–1.32)	<0.01	0.77 (0.59–1.32)
11 Former USSR (0.151)	19.8 (11.36–24.38)	2.08 (1.58–2.56)	21.88 (12.94–26.94)	7.73 (3.96–9.65)	0.76 (0.51–0.96)	8.49 (4.47–10.61)	13.36 (7.58–16.45)	1.49 (1.13–1.81)	14.85 (8.71–18.26)
12 Middle East (0.082)	0.91 (0.13–4.63)	0.04 (<0.01–0.04)	0.95 (0.13–4.67)	0.74 (0.23–3.38)	0.06 (<0.01–0.06)	0.8 (0.23–3.44)	0.79 (0.17–3.71)	0.04 (0–0.04)	0.83 (0.17–3.75)
13 South Asia (0.101)	1.03 (0.65–2.16)	0.08 (0.04–0.13)	1.1 (0.68–2.29)	1.51 (0.98–2.49)	0.1 (0.05–0.14)	1.61 (1.03–2.63)	1.14 (0.74–2.08)	0.08 (0.04–0.12)	1.22 (0.77–2.2)
14 East Asia (0.467)	13.12 (10.21–15.55)	0.46 (0.38–0.62)	13.59 (10.6–16.17)	4.65 (3.46–6.06)	0.17 (0.11–0.34)	4.81 (3.57–6.4)	8.61 (6.69–10.33)	0.34 (0.27–0.49)	8.95 (6.96–10.82)
15 Southeast Asia (0.143)	0.63 (0.44–1.11)	0.01 (0.01–0.13)	0.64 (0.45–1.24)	0.13 (0.09–0.22)	<0.01 (<0.01–0.04)	0.13 (0.09–0.26)	0.39 (0.28–0.67)	0.01 (0.01–0.1)	0.4 (0.29–0.78)
16 Oceania (0.031)	8.78 (5.3–10.4)	0.57 (0.21–0.77)	9.35 (5.51–11.17)	9.43 (5.31–11.65)	0.59 (0.22–0.88)	10.02 (5.53–12.53)	9.07 (5.27–10.82)	0.55 (0.21–0.78)	9.62 (5.48–11.6)
17 Japan (0.122)	<0.01	<0.01	<0.01	<0.01	<0.01	<0.01	<0.01	<0.01	<0.01

Table 3
Statistics of model-derived (runs 2 × 2.5 and 1.5 × 1.5) 100-m wind speeds versus sounding-derived (http://www.esrl.noaa.gov/raobs) and MERRA-derived (Rienecker et al., 2012) wind speeds extrapolated to 100 m with the Least Square Error method (Archer & Jacobson, 2003, 2005) at sounding locations that are relevant for practical wind power (i.e., with average 100-m wind speed > 7 m/s).

Month	N. sites	Average (m/s)				Standard deviation (m/s)				Bias (m/s)			RMSE (m/s)			NGE (fraction)		
		Obs	2 × 2.5	1.5 × 1.5	MERRA	Obs	2 × 2.5	1.5 × 1.5	MERRA	2 × 2.5	1.5 × 1.5	MERRA	2 × 2.5	1.5 × 1.5	MERRA	2 × 2.5	1.5 × 1.5	MERRA
Jan	135	8.77	8.27	7.65	7.91	1.55	2.29	2.15	1.77	−0.50	−1.12	−0.86	2.28	2.37	1.49	0.20	0.22	0.13
Feb	134	8.63	8.20	7.53	8.04	1.69	2.26	1.62	1.78	−0.43	−1.10	−0.59	2.52	2.55	1.52	0.23	0.21	0.14
Mar	132	8.46	8.23	7.57	7.68	1.57	2.05	1.72	1.72	−0.23	−0.89	−0.78	1.91	2.01	1.30	0.18	0.18	0.12
Apr	93	8.63	7.61	7.28	7.82	1.60	2.10	1.67	1.76	−1.02	−1.35	−0.80	1.75	2.24	1.49	0.16	0.19	0.14
May	75	8.45	7.78	6.92	7.53	1.43	2.68	2.24	1.69	−0.67	−1.53	−0.91	1.81	2.23	1.41	0.17	0.22	0.13
Jun	70	8.49	8.00	7.10	7.87	1.51	3.56	3.57	1.96	−0.49	−1.39	−0.63	3.05	3.35	1.39	0.26	0.30	0.14
Jul	72	8.79	8.50	7.61	8.00	1.56	4.10	3.01	2.11	−0.29	−1.18	−0.79	3.39	2.75	1.73	0.29	0.25	0.16
Aug	62	8.50	8.42	7.50	7.84	1.39	3.72	3.87	1.75	−0.08	−1.00	−0.66	2.82	3.41	1.43	0.26	0.30	0.14
Sep	69	8.69	8.03	7.45	7.89	1.65	3.04	2.70	1.93	−0.67	−1.24	−0.80	2.52	2.51	1.66	0.22	0.22	0.15
Oct	103	8.60	8.02	7.09	7.81	1.68	2.04	2.03	1.75	−0.58	−1.51	−0.79	1.74	2.56	1.45	0.16	0.23	0.13
Nov	126	8.36	7.95	7.42	7.74	1.37	1.99	1.51	1.66	−0.40	−0.94	−0.62	2.01	2.16	1.20	0.18	0.18	0.11
Dec	132	8.50	7.95	7.70	7.83	1.36	1.87	1.91	1.58	−0.55	−0.80	−0.67	2.13	2.40	1.31	0.20	0.20	0.12
Year		8.57	8.08	7.40	7.83	1.53	2.64	2.33	1.79	−0.49	−1.17	−0.74	2.33	2.55	1.45	0.21	0.23	0.13

Validation

In this study we used the same model as in Jacobson and Archer (2012), who found that it compared adequately with QuikSCAT data over the oceans at a model resolution of 4° × 5°. They found that the model results matched the magnitude and location of the "roaring 40s" in the Southern Hemisphere (SH) and locations of the Northern-Hemisphere (NH) mid-latitude westerlies. The magnitudes of the westerlies were slightly underpredicted, suggesting that wind power estimates over the ocean there could be slightly underpredicted. The model also generally underestimated wind speeds along the tropics, in the middle latitudes in both hemispheres, and along some coastal regions.

Here, we further compare the model 100-m wind speeds from runs 2° × 2.5° and 1.5° × 1.5° with three additional sources of data:

1. Soundings: wind speeds measured at all sounding stations worldwide (http://www.esrl.noaa.gov/raobs/) were interpolated to 100 m with the Least Square Error (LSE) method (Archer & Jacobson, 2003, 2005) applied to the lowest three sounding levels. In brief, the LSE method tries six fitting profiles through the three observed wind speeds and heights and selects the one with the lowest mean square error to determine the 100-m wind speed. The method has been validated against observed meteorological tower data at the Kennedy Space Center and it is generally very accurate, with an average error of −3.2% (Archer & Jacobson, 2005).
2. MERRA reanalyses: wind speeds at 0.5° × 0.667° horizontal resolution (Rienecker et al., 2012) for 2008 are available every 6 h on 72 vertical sigma-p levels, whose heights above ground vary each time. Wind speeds on the lowest three sigma-p levels, corresponding to average pressures of approximately 977, 962, and 947 hPa, were interpolated to 100 m with the Least Square Error method (Archer & Jacobson, 2003, 2005) after calculating their heights above ground at all points using actual virtual temperature and the hydrostatic assumption;
3. a higher-resolution run of GATOR-GCMOM (0.5° × 0.75°) limited to the U.S. only.

Table 3 summarizes the validation. Because this study focuses on the practical wind potential, the validation is performed at sounding locations with monthly-average wind speed at 100 m > 7 m/s. Overall the GATOR-GCMOM model performed satisfactorily and conservatively, with a negative bias in both runs (−0.49 and −1.17 m/s from runs 2 × 2.5 and 1.5 × 1.5 respectively). The MERRA reanalyses too had a negative bias of −0.74 m/s. As such, the results in this study are overall unlikely to over-estimate the practical wind power potentials. The

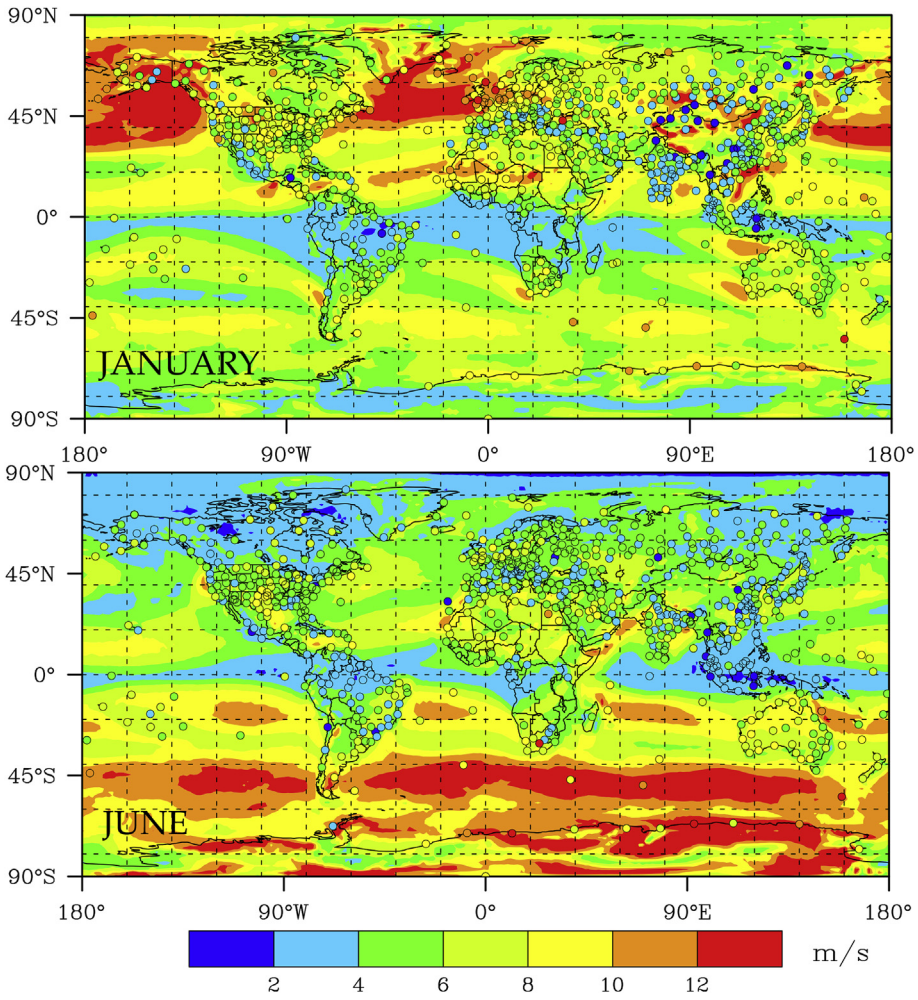

Fig. 8. Comparison of simulated 100-m wind speed (shaded colors) with data (filled circles) from ~600 soundings (http://www.esrl.noaa.gov/raobs) in January and June 2008 extrapolated to 100 m using the Least Square Error method (Archer & Jacobson, 2003, 2005). (For interpretation of the references to color in this figure legend, the reader is referred to the web version of this article.)

2° × 2.5° run had a slightly better performance overall than the 1.5° × 1.5° run (in terms of bias, root-mean square error RMSE and normalized gross error NGE), mainly because it produced slightly higher winds overall. The MERRA reanalyses had better NGE and RMSE than both GATOR-CGMOM runs, likely because sounding data were assimilated directly in them. As such, we conclude that, despite the lower resolution and lack of data assimilation, GATOR-CGMOM had a similar performance as the MERRA reanalyses for locations that are relevant for practical wind power potential.

Fig. 8 shows global maps of simulated and observed 100-m wind speeds during two months (January and June 2008) from the 1.5° × 1.5° run. The model reproduces remarkably well the observed distributions, especially over the U.S. and Europe, where the sounding stations are numerous and generally well maintained. The exception is a persistent over-estimate over India and Southeast Asia, perhaps due to difficulties in dealing with tropical convection. However, these locations generally have weak winds and were not included in the practical wind power potential calculation (Fig. 4).

Lastly, to verify that increasing resolution improves accuracy without altering overall results, a high-resolution run (0.5° × 0.75°) of the GATOR-GCMOM was conducted over the U.S. only. Due to its high computational requirements, it was run for only three months of 2006 (January–March). Out of the 91 sounding sites available in the US, only 20–32 had monthly-average 100-m wind speeds > 7 m/s and were used for the comparison. During the three months, the bias was 0.25 m/s; the RMSE, 1.15 m/s; and the NGE, 15.4%, all of which are better than the corresponding statistics for the 2° × 2.5° and the 1.5° × 1.5°, although for a different year. This suggests that higher-resolution improves model accuracy. However, the geographic distributions of wind speed were qualitatively similar to those of the lower-resolution runs and the sounding locations with the largest under- and over-estimates coincided in all runs, which suggests that not even at 0.5° × 0.75° was it possible to capture all local effects. We conclude that global results from GATOR-GCMOM at 1.5° × 1.5° are satisfactory for practical wind power calculations.

Implications and conclusions

The wind resource analysis here suggests that global practical wind power is abundant and spatially distributed. Practical wind power locations, which are areas that meet all practical requirements for wind installations (sufficient wind, low elevation or bathymetry, and compatible land use, with all system losses included), cover ~30% of all land and near-shore areas outside of polar regions worldwide. More high-wind areas are found over land in the Northern Hemisphere than in the Southern Hemisphere. However, the global practical wind power potential varies significantly with season and hemisphere. Net capacity factors in excess of 0.4 are hard to find on Earth based on yearly-average and somewhat coarse-resolution maps, but are not uncommon during selected seasons. Even though regional practical wind resources are sensitive to several imposed assumptions (e.g., how windy a site needs to be or at what depth an offshore wind farm can be built), they greatly exceed regional demands for electricity, except in Japan. The GATOR-GCMOM model at 1.5° × 1.5° resolution predicts global winds satisfactorily compared with high-resolution MERRA reanalyses and with observed soundings at practical wind power locations.

An implication of this work is that information based on yearly-averages is not sufficient to estimate wind farm performance during individual seasons because the frequency distributions and the geographical patterns in each season are often dramatically different from the yearly-average ones.

References

Adams, A. S., & Keith, D. W. (2013). Are global wind power resource estimates overstated? *Environmental Research Letters, 8*(1), 015021. http://dx.doi.org/10.1088/1748-9326/8/1/015021.

Arakawa, A., & Lamb, V. R. (1981). A potential enstrophy and energy conserving scheme for the shallow water equations. *Monthly Weather Review*, 18–36.

Archer, C. L., & Jacobson, M. Z. (2003). Spatial and temporal distributions of U.S. winds and wind power at 80 m derived from measurements. *Journal of Geophysical Research, 108*(D9). http://dx.doi.org/10.1029/2002JD002076.

Archer, C. L., & Jacobson, M. Z. (2005). Evaluation of global wind power. *Journal of Geophysical Research, 110*(D12). http://dx.doi.org/10.1029/2004JD005462.

Arya, S. P. (1988). *Introduction to micrometeorology*. Academic Press.

Burton, T., Sharpe, D., Jenkins, N., & Bossanyi, E. (2001). *Wind energy handbook*. John Wiley and Sons.

Capps, S. B., & Zender, C. S. (2010). Estimated global ocean wind power potential from QuikSCAT observations, accounting for turbine characteristics and siting. *Journal of Geophysical Research, 115*(D9). http://dx.doi.org/10.1029/2009JD012679.

Cho, A. (2010). Energy's tricky tradeoffs. *Science, 329*, 786–787.

Dee, D., Uppala, S., & Simmons, A. (2011). The ERA-interim reanalysis: configuration and performance of the data assimilation system. *Quarterly Journal of the Royal Meteorological Society, 137*, 553–597.

Dvorak, M. J., Archer, C. L., & Jacobson, M. Z. (2010). California offshore wind energy potential. *Renewable Energy, 35*(6), 1244–1254. http://dx.doi.org/10.1016/j.renene.2009.11.022.

Dvorak, M. J., Stoutenburg, E. D., Archer, C. L., Kempton, W., & Jacobson, M. Z. (2012). Where is the ideal location for a US East Coast offshore grid? *Geophysical Research Letters, 39*(6) http://dx.doi.org/10.1029/2011GL050659.

EIA. (2011, May). Energy information administration – frequently asked questions. Retrieved 26.06.12, from http://tonto.eia.doe.gov/tools/faqs/faq.cfm?id=105&t=3.

Frandsen, S. (2007). *Turbulence and turbulence-generated structural loading in wind turbine clusters* (No. R-1188(EN)) (pp. 1–135). Roskilde, Denmark: Riso National Laboratory.

GEA. (2012). In IIASA (Ed.), *Global energy assessment – Toward a sustainable future*. Cambridge University Press.

GFS. (2010). Global forecast system – 1° × 1° reanalysis fields. Retrieved 26.06.12, from http://nomads.ncdc.noaa.gov/data/gfs-avn-hi.

Grubb, M. J., & Meyers, N. I. (1993). *Wind energy: Resources, systems, and regional strategies* (pp. 157–212). Island Press.

Hoogwijk, M., de Vries, B., & Turkenburg, W. (2004). Assessment of the global and regional geographical, technical and economic potential of onshore wind energy. *Energy Economics, 26*(5), 889–919. http://dx.doi.org/10.1016/j.eneco.2004.04.016.

International Energy Agency. (2012). *Key world energy statistics 2012* (pp. 1–82). IEA.

Jacobson, M. Z. (2001). GATOR-GCMM: a global through urban scale air pollution and weather forecast model. 1. Model design and treatment of subgrid soil, vegetation, roads, rooftops, water, sea ice, and snow. *Journal of Geophysical Research, 106*, 5385–5402.

Jacobson, M. Z. (2010). Short-term effects of controlling fossil-fuel soot, biofuel soot and gases, and methane on climate, Arctic ice, and air pollution health. *Journal of Geophysical Research, 115*(D14209). http://dx.doi.org/10.1029/2009JD013795.

Jacobson, M. Z., & Archer, C. L. (2012). Saturation wind power potential and its implications for wind energy. *Proceedings of the National Academy of Sciences of the United States of America, 109*(39), 15679–15684. http://dx.doi.org/10.1073/pnas.1208993109.

Jacobson, M. Z., & Delucchi, M. A. (2011). Providing all global energy with wind, water, and solar power, part I: technologies, energy resources, quantities and areas of infrastructure, and materials. *Energy Policy, 39*(3), 1154–1169. http://dx.doi.org/10.1016/j.enpol.2010.11.040.

Jacobson, M. Z., & Masters, G. M. (2001). Exploiting wind versus coal. *Science, 293*, 1438.

Jacobson, M. Z., & Streets, D. G. (2009). Influence of future anthropogenic emissions on climate, natural emissions, and air quality. *Journal of Geophysical Research, 114*(D8). http://dx.doi.org/10.1029/2008JD011476.

Jiang, Q., Doyle, J. D., Haack, T., Dvorak, M. J., Archer, C. L., & Jacobson, M. Z. (2008). Exploring wind energy potential off the California coast. *Geophysical Research Letters, 35*(20). http://dx.doi.org/10.1029/2008GL034674.

Keith, D. W., DeCarolis, J. F., Denkenberger, D. C., Lenschow, D. H., Malyshev, S., Pacala, S., et al. (2004). The influence of large-scale wind power on global climate. *Proceedings of the National Academy of Sciences of the United States of America, 101*(46), 16115–16120.

Ketefian, G. S., & Jacobson, M. Z. (2009). A mass, energy, vorticity, and potential enstrophy conserving lateral fluid–land boundary scheme for the shallow water equations. *Journal of Computational Physics, 228*(1), 1–32. http://dx.doi.org/10.1016/j.jcp.2008.08.009.

Liu, W. T., Tang, W., & Xie, X. (2008). Wind power distribution over the ocean. *Geophysical Research Letters, 35*(13). http://dx.doi.org/10.1029/2008GL034172.

Lu, X., McElroy, M. B., & Kiviluoma, J. (2009). Global potential for wind-generated electricity. *Proceedings of the National Academy of Sciences of the United States of America*, 1–6. http://dx.doi.org/10.1073/pnas.0904101106.

Marvel, K., Kravitz, B., & Caldeira, K. (2012). Geophysical limits to global wind power. *Nature Climate Change, 2*(9), 1–4. http://dx.doi.org/10.1038/nclimate1683.

Masters, G. M. (2005). *Renewable and efficient electric power systems*. John Wiley and sons.

Rienecker, M. M., Suarez, M. J., Gelaro, R., Todling, R., Bacmeister, J., Liu, E., et al. (2012). MERRA: NASA's modern-era retrospective analysis for research and applications. *Journal of Climate, 24*(14), 3624–3648. http://dx.doi.org/10.1175/JCLI-D-11-00015.1.

Zhang, Y. (2008). Online-coupled meteorological and chemistry models: history, current status, and outlook. *Atmospheric Chemistry and Physics, 8*, 2895–2932.